Journal of Materials Chemistry

Cite this: J. Mater. Chem., 2012, 22, 21667

www.rsc.org/materials

PAPER

Layer by layer assembly of heparin/layered double hydroxide completely renewable ultrathin films with enhanced strength and blood compatibility†

Yingqi Shu,[a] Penggang Yin,*[b] Benliang Liang,[b] Shasheng Wang,[b] Longcheng Gao,[b] Hao Wang*[a] and Lin Guo*[b]

Received 18th July 2012, Accepted 25th August 2012
DOI: 10.1039/c2jm34728h

Renewable nacre-like heparin (HEP)/layered double hydroxide (LDH) ultrathin films were first fabricated *via* a bottom-up layer by layer (LBL) deposition technique, which simultaneously showed largely enhanced mechanical properties and good blood compatibility. The results of UV-vis, FTIR, XRD and SEM analysis indicate that the HEP/LDH ultrathin films stacked densely together to form a well-defined brick-and-mortar structure. A strong electrostatic and hydrogen bond network at the organic–inorganic interface allowed the modulus of the film reach *ca.* 23 GPa, which was remarkably enhanced compared to previously reported polymer–LDH hybrid films. Due to the interlamellar heparin, the $(HEP/LDH)_n$ film may prove to be beneficial for new medical applications or as a replacement for conventional petroleum based plastics.

Introduction

Systematic studies are carried out in materials science on natural materials with the objective of duplicating their properties in artificial materials. Seashell nacre is well known for its distinctive mechanical qualities due to its highly regular brick-and-mortar arrangement of organic and inorganic elements, which has inspired a large class of biomimetic advanced materials[1–4] and organic–inorganic composites.[5–12] Although substantial progress has been made on mimicking the micro- and nanostructures of nacre, the manufacture of artificial composites that copy nature's designs remains a challenging goal. Due to the indispensability of platelet-like inorganic materials in the biomimetic composites, in previous reports,[7,13–16] the clay and Al_2O_3 platelets were just used to reinforce the polymer matrix without bringing other functionalities to these artificial materials.

Layered double hydroxides (LDH) have the advantages of renewability, facile preparation, low cost, good biocompatibility and low cytotoxicity. They have been employed as additives to enhance the mechanical,[17] optical,[18] catalytic,[19] and fire-retardant properties[20] of composites. However, using LDHs as the inorganic bricks in the fabrication of biologically inspired organic–inorganic hybrid films has been rarely reported. Compared with the flexible chain structure of polyelectrolytes, LDH monolayers are rigid and crystalline.[21] Up until now, some LDHs have been exfoliated into positively charged monolayers[10,17,22] that can be assembled alternately with polyanions into thin films. Although the mechanical properties of these composites were enhanced compared to the pure polymer matrix or inorganic phase, this improvement is still fall far below that of natural materials. Therefore, there is an urgent demand to develop new types of biomimetic materials with high hierarchical orientation and strong bonding at the inorganic–organic interface.

Heparin (HEP) is a natural anionic polysaccharide, which is well-known for its anticoagulant activity and for having the highest negative charge density of all biological polyanions. Herein, the HEP molecules are easily coated onto exfoliated LDH nanosheets to yield completely renewable artificial HEP/LDH hybrid films. A strong electrostatic and hydrogen bond network at the organic–inorganic interface aims to recreate a biologically inspired nacre-like nanostructure.

Herein, we fabricated the hybrid composite by bottom-up LBL assembly of HEP with LDHs, which, for the first time, resulted in novel nacre-like $(HEP/LDH)_n$ ultrathin films. The hybrid films achieved high strength (modulus up to 23 GPa) and are also endowed with good blood compatibility. The environmentally benign HEP/LDH nanocoatings could prove to be beneficial for new types of medical application or as a replacement of conventional petroleum based plastics.

Experimental

Materials

The following analytical grade reagents were purchased from Sinopharm Chemical Reagent Co. Ltd and used as received: heparin (HEP, M_w = 6–20 kD), $Ni(NO_3)_2 \cdot 6H_2O$,

[a]*The College of Materials Science and Engineering Department of Chemistry, Beijing University of Technology, Beijing, 100124, China. E-mail: haowang@bjut.edu.cn; Fax: +86-010-67390966; Tel: +86 86-010-67390966*
[b]*School of Chemistry & Environment, Beihang University, Beijing, 100191, China. E-mail: pgyin@buaa.edu.cn; guolin@buaa.edu.cn; Fax: +86-010-82338162; Tel: +86-010-82338162*

† Electronic supplementary information (ESI) available: more PUL results. See DOI: 10.1039/c2jm34728h

$Al(NO_3)_3 \cdot 9H_2O$, NaOH, H_2O_2, H_2SO_4, HCl. Silane coupling agent 3-aminopropyltriethoxysilane (ATES) was purchased from Aldrich Co.

Preparation of exfoliated NiAl–LDH nanosheets

In a typical procedure, $Ni(NO_3)_2 \cdot 6H_2O$ (0.016 mol), $Al(NO_3)_3 \cdot 9H_2O$ (0.008 mol) were dissolved in 20 ml of deionized water to give the final concentrations of 8 and 4 mM, respectively. NaOH solution was then added dropwise into the solution until it reached the appointed constant pH while the solution was stirred by a magnetic stirrer. The mixture was sealed in a teflon-lined stainless steel autoclave and heated at 180 °C for 12 h. The resulting green, solid product was filtered, washed with deionized water and anhydrous ethanol several times, and finally air-dried at 70 °C for 4 h. The exfoliated, positively charged LDH nanosheets were synthesized by vigorously agitating 0.1 g of Ni–Al–NO_3 LDH in 100 ml of formamide in a two-neck flask under a N_2 gas flow for 24 h.

HEP/LDH ultrathin film fabrication

Multilayer ultrathin films of the unilamellar LDH nanosheets/HEP were fabricated by applying the layer-by-layer assembly procedure. Substrates, such as a silicon wafer and quartz, were cleaned by immersion into hot "piranha" solution (1 : 3 H_2O_2 : H_2SO_4) for 30 min, followed by thoroughly rinsing with deionized water and anhydrous ethanol several times, and dried under a flow of nitrogen. The substrates were then modified with 3-aminopropyltriethoxysilane (ATES) by heating to reflux in toluene that contained 5 wt% ATES for at least 6 h to obtain chemically bonded $-NH_2$ groups on the surface. The surface was rinsed with toluene and dichloromethane to remove any remaining ATMS, dried under a flow of nitrogen gas, and immersed in dry dichloromethane that contained pyridine (2% v/v). A positive surface charge was induced by dipping the substrate in HCl (pH ≈ 1–2) before starting the deposition.

First, the pretreated substrate was dipped into a HEP aqueous solution (1.0 g ml^{-1}) for 10 min, followed by rinsing with copious amounts of deionized water. The substrate treated with negatively charged HEP was then immersed into the colloidal LDH suspension (1.0 g ml^{-1}) containing NiAl–LDH nanosheets for 10 min and washed with water afterwards. Subsequently, a series of alternative deposition operations for HEP and LDH nanoplatelets was repeated n times to produce multilayer films of $(HEP/LDH)_n$ (Scheme 1). The final films were dried with a nitrogen gas flow.

Blood compatibility test

Hemolysis ratio. In order to test the hemolysis ratio of the samples, blood was drawn from healthy donors, containing 3.2% sodium citrate. All experiments of blood compatibility were performed in compliance with the relevant laws and institutional guidelines. The Ethical Committee of Beijing University of Technology approved these experiments. 4 ml of blood was diluted by 5 ml of 0.9% (weight/volume, w/v) sodium chloride solution. Every testing sample was split into equal volumes and added into 10 ml of 0.9% (w/v) sodium chloride solution. All of the samples were kept at 37 °C for 30 min, and immediately thereafter, were

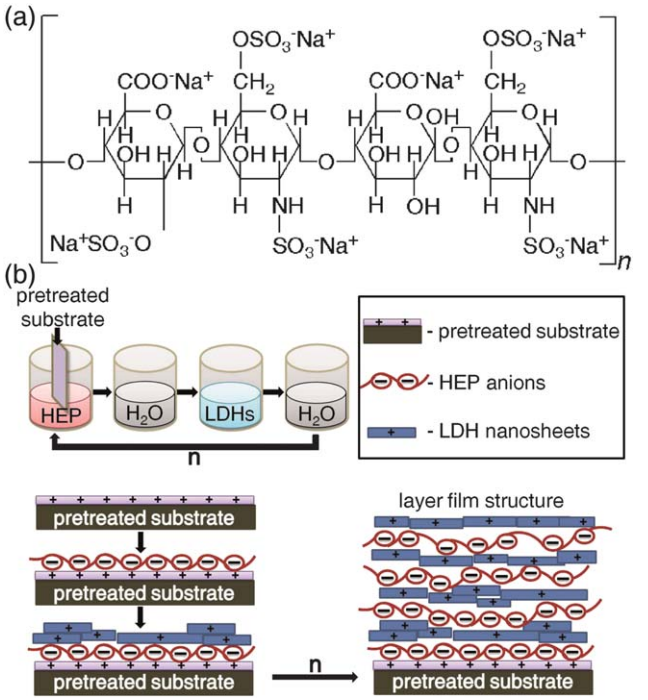

Scheme 1 (a) Chemical structure of HEP. (b) Fabrication of the artificial nacre-like $(LDH/HEP)_n$ bio-nanocomposite film.

incubated with 0.2 ml of the whole blood. Additionally, positive and negative controls were obtained by adding 0.2 ml of human blood to 10 ml of double distilled water and 0.9% sodium chloride solution, respectively. After incubation for 60 min, the samples were centrifuged at 2000 rpm for 5 min. The percent hemolysis was calculated by measuring the absorbance of the supernatant solution at 540 nm in a UV-vis spectrophotometer. The hemolysis ratio was calculated as follow: $R = (A - C^1)/(C^2 - C^1) \times 100\%$, where R is the hemolysis ratio (%), A is the absorbency of the sample (%), C^1 is the absorbency of the negative controls (%), and C^2 is the absorbency of the positive control (%).

Dynamic clotting time experiment. The *in vitro* thrombo resistant properties were evaluated with human acid citrate dextrose (ACD) blood using the kinetic method investigated by Imai and Nose[23] improved by Komai and Nose.[24,25] The $(HEP/LDH)_{300}$ films were cut into small pieces and the samples were equilibrated in normal saline water. 0.2 ml anticoagulated blood (ACD: blood, 4 : 1) from human volunteers was added to each $(HEP/LDH)_{300}$ film surface in an open atmosphere at 37 °C. The coagulate reaction was then initiated by dropping 0.02 ml of 0.2 M calcium chloride solution on each specimen of blood. After a predetermined time (10, 20, 30, 40, 50 and 60 min), the blood on the test surface was transferred into a beaker containing 50 ml of double distilled water. The optical density of the supernatant was then measured at 540 nm wavelengths using a UV-vis spectrometer. The relationship between the optical density and time was plotted as the clotting time curves.

Nanomechanical test

Due to the very low thickness of the ultra-thin film, we use the $(HEP/LDH)_{300}$ film performed at shallow indentation depth to

avoid or limit the effect of the silicon substrate. The Hysitron nanoindenter monitors and records the load and displacement of the indenter. A general rule of thumb when testing thin films is to test only the first 10–20% of the film thickness to avoid the effect of the substrate on the measurements. Prior to testing, the specimen was imaged *in situ* using the nanoindentation tip as a scanning probe microscope (SPM) to ensure that the location for the indent was clean and relatively flat. Once the desired position was defined, we use two patterns to obtain the mechanical properties of the $(HEP/LDH)_{300}$ sample.

Indentation test. Eight load-controlled indentation tests were performed on the sample to determine the hardness and reduced modulus. Eight indents were performed on the sample, with peak indentation loads of 100 μN for the $(HEP/LDH)_{300}$ films. Each indent consisted of a five-second loading and a five-second unloading.

PUL test. PUL is useful for verification that thin film measurements are free of the substrate effect by observing local minima or maxima in the measured properties prior to observation of substrate influence. Three partial-unloading indents were performed on the film. These indents consisted of 66 cycles of loading with a progressively increasing load. Each cycle included a one-second loading, a one-second hold, and a one-second unloading. The peak loads were 100 μN for the 530 nm thickness of the $(HEP/LDH)_{300}$ film. The unloading segments of each indent were then analyzed to determine hardness and reduced modulus. Similar to the analysis of the single-cycle nanoindentation data, depth profiling nanoindentation results can be ranked according to measured mechanical properties.

Characterization

X-Ray diffraction (XRD) data of $(HEP/LDH)_n$ films were recorded by a Shimadzu XRD-6000 diffractometer under the following conditions: 40 kV, 30 mA, Cu Kα radiation. Fourier transform infrared (FT-IR) spectra were measured on a Nicolet NEXUS-470 infrared spectrophotometer using the KBr pellet technique. UV-vis absorption spectra were recorded in the range from 190 to 300 nm on a Shimadzu-3600 spectrophotometer, and the slit width was 1.0 nm. The morphology and dimension of the samples were examined with a HITACHI S4800 scanning electron microscope (SEM), operating at an accelerating voltage of 5 kV. Transmission electron microscopy (TEM) was performed using a JEOL JEM-2100F transmission electron microscope at an acceleration voltage of 200 kV. A Bruker atomic force microscope (AFM) was used to examine the surface topography of the films deposited on Si wafers. The mechanical properties of the LBL films were tested using the HYSITRON TI-950 Tribolndenter, where a Berkovoich shape indenter was used. TI-950 Tribolndenter works well for thin films greater than approximately 200 nm in thickness. The hardness and Young's modulus were calculated and recorded.

Results and discussion

Exfoliation of LDHs

Fig. 1a shows an XRD pattern of the green product that was prepared by the $Ni(NO_3)_2$–$Al(NO_3)_3$–NaOH system. The sharp and symmetric features of the diffraction peaks strongly suggest that the produced Ni–Al–NO_3 LDH was highly crystallized with a three-dimensional order. The d_{003} represented the interlayer distance (8.8 Å) in the layered double hydroxide structure, which confirmed the formation of the nitrate form of the LDH. Intercalation of NO_3^- anions was confirmed by FT-IR spectra (Fig. 1b). The sharp and strong absorption peak at 1384 cm^{-1} shown in Fig. 1b is attributed to the N–O stretching vibration mode of NO_3^- anions.

Fig. 2a and b show representative tapping AFM images of delaminated two-dimensional ultrathin Ni–Al LDH sheets deposited on a silicon substrate. We observe a thin layer of dispersed nanoparticles lying on the substrate surface. The height profile scan revealed that the nanosheets had a fairly flat terrace with an average thickness of 0.80 ± 0.05 nm. The thickness was measured at a step between a nanosheet and the substrate surface and between a nanosheet and another nanosheet overlapped on it. The theoretical thickness of the LDH sheet is 0.48 nm.[26,27] Possible adsorption of formamide as well as counteranions, *e.g.*, NO_3^- or CO_3^{2-}, on the nanosheet surface may be responsible for the deviation of *ca.* 0.30 nm. In any case, such a thickness unambiguously indicated that the nanosheets were unilamellar. TEM images also revealed the morphology of the obtained suspension, as shown in Fig. 2c, where some nanosheets were not completely delaminated or were aggregated delaminated single or double nanosheets. When the as-prepared Ni–Al–NO_3 LDH nanosheets were treated with formamide, a transparent green colloidal suspension (see Fig. 2c inset) was yielded, suggesting that delamination had occurred. Tyndall light scattering was clearly observed, indicating the presence of exfoliated LDH layers dispersed in the formamide. The resulting colloidal solution was very stable, and no sediment was observed upon long-term storage.

Frabrication of nacre-like $(HEP/LDH)_n$ ultrathin films

Multilayer $(HEP/LDH)_n$ films were obtained by alternately dipping a silicon slide into a colloidal suspension of the LDH nanosheets and a HEP solution. The growth of LDH/HEP multilayer films was monitored by UV-vis absorption spectra measured immediately after every ten deposition cycles (Fig. 3a). The intensity of the absorption band around 195 nm of HEP increased linearly with the number of bilayers *n* (Fig. 3b), which indicated a stepwise and regular ultrathin film deposition procedure. From the FTIR spectra (Fig. 3c), the LDH feature peaks could still be observed after being assembled with HEP anions, but the O–H bands became broader and NO_3^- bands

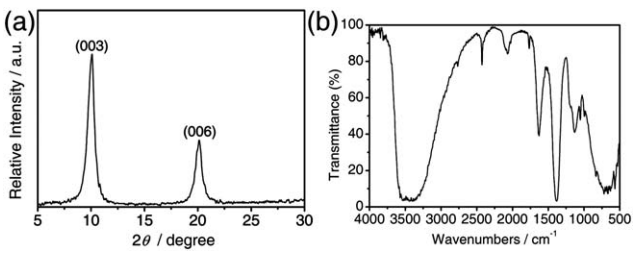

Fig. 1 (a) XRD pattern of the as-prepared Ni–Al–NO_3 LDH sample. (b) Powder FTIR spectrum.

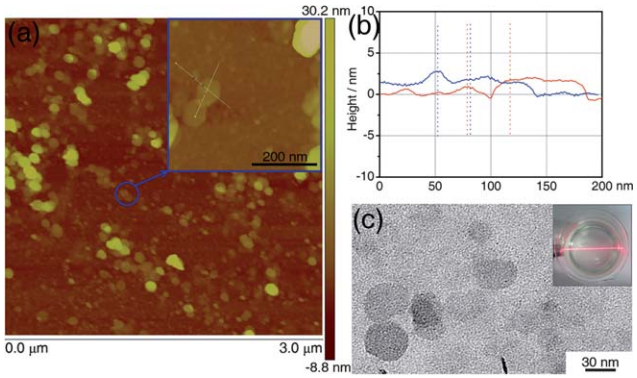

Fig. 2 (a) Tapping AFM image of the exfoliated LDH nanosheets deposited on a Si wafer substrate. (b) Height profile along the marked line in (a). (c) TEM patter of LDH nanosheets (inset: photograph of a colloidal suspension of exfoliated Ni-Al LDH nanosheets).

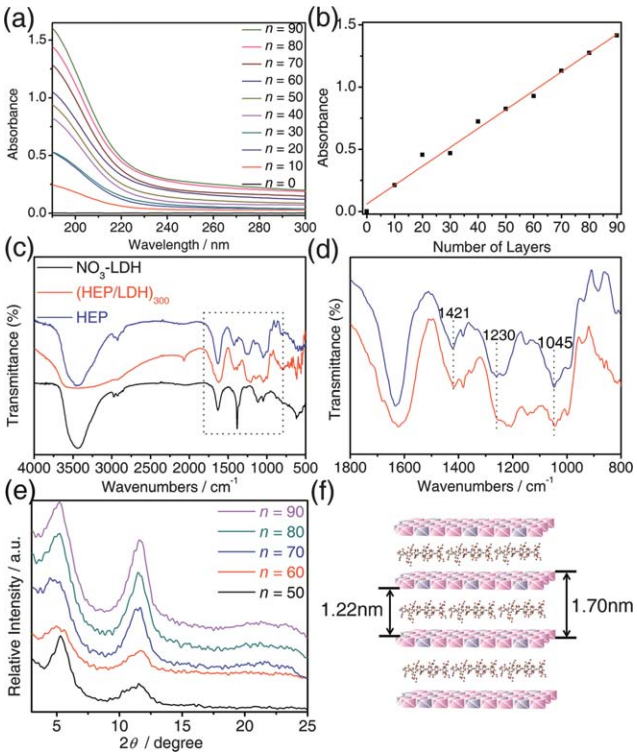

Fig. 3 (a) UV-vis absorption spectra of multilayer film of $(LDH/HEP)_n$ assembled on a quartz glass substrate. (b) The absorbance at 195 nm *versus* the number of deposition cycles. (c) FTIR spectrum of the $(HEP/LDH)_{300}$ film. (d) Close up of the spectrum in (c). (e) XRD patterns for the multilayer assembly of $(LDH/HEP)_n$. (f) Structure model for the HEP/Ni-Al LDH system.

became much weaker. A few characteristic bands of HEP were observed (Fig. 3d) when the $(HEP/LDH)_{300}$ ultrathin film was compared with heparin sodium salt. These bands were assigned to the stretching vibration of C=O symmetric stretching (1421 cm^{-1}, C=O st_s), S=O antisymmetric (1230 cm^{-1}, S=O st_{as}) and symmetric stretching vibration (1045 cm^{-1}, S=O st_s). XRD patterns (Fig. 3e) of the multilayer films exhibited a Bragg diffraction peak at *ca.* 5.1°, which was attributable to a so-called superlattice reflection of the inorganic–organic repeating nanostructure. Its enhancement with increasing numbers of deposition cycles indicated the progressive growth of the assembled nanostructure. The peak at *ca.* 5.1° corresponded to the $d_{003} \approx$ 1.7 nm of the $(LDH/HEP)_n$ ultrathin films, demonstrating the films have long range stacking order in the normal direction of the substrate. Allowing for a thickness of about 0.48 nm for the LDH nanosheets, the layer height of HEP along the film normal was estimated to be about 1.2 nm (Fig. 3f).

Fig. 4a–c shows the cross-sectional morphologies of $(LDH/HEP)_{100}$, $(LDH/HEP)_{200}$, $(LDH/HEP)_{300}$ multilayer films. $(LDH/HEP)_n$ hybrid films were stacked densely together to form a well-defined layered structure, resembling the brick-and-mortar structure of nacre. SEM images illustrated the dependence of the thickness of the HEP/LDH thin films on the value of n. The thickness was 0.18 ± 0.1, 0.34 ± 0.1 and 0.53 ± 0.1 μm obtained from a side view image, where the corresponding bilayers of LDH/HEP were 100, 200 and 300, respectively. The linear increase of the thickness upon increasing bilayer number confirmed that the ultrathin film presented a uniform and periodic layered structure. The thickness of one bilayer in the LDH/HEP film was estimated to be *ca.*1.8 nm, which was in agreement with the thickness per deposited cycle observed by XRD. The top-view SEM images (Fig. 4d) showed that the surface of the $(HEP/LDH)_{300}$ film was microscopically smooth and uniform, as the LDH nanoplatelets were glued together by the HEP. The thin film could be clearly observed on the silicon substrate.

Blood compatibility of the $(HEP/LDH)_n$ ultrathin film

Heparin is an anionic polysaccharide that has been extensively used in medicine due to its good blood compatibility and low toxicity. In order to evaluate the effectiveness of the $(HEP/LDH)_n$ film on blood compatibility, preliminary hemolysis tests and *in vitro* dynamic clotting time assessments were conducted. Hemolysis of the blood is a problem associated with bio-incompatibility.[28] Hemolysis occurs when cells swell to the critical bulk to burst the cell membranes. Red blood cells hemolyse when they come into contact with water. This problem

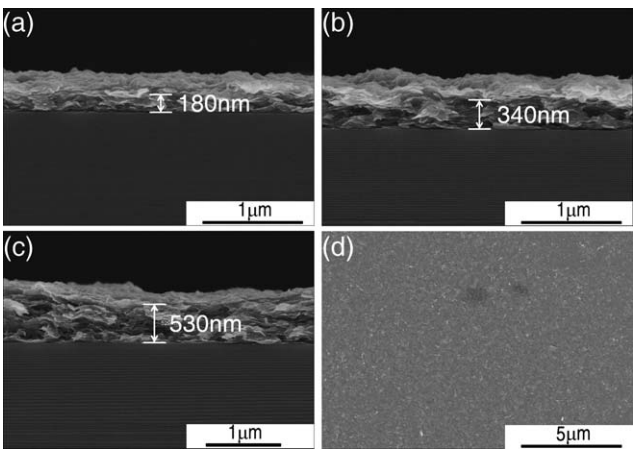

Fig. 4 Cross-sectional SEM images of different films. (a) $(HEP/LDH)_{100}$. (b) $(HEP/LDH)_{200}$. (c) $(HEP/LDH)_{300}$. (d) Top view of SEM image for the $(HEP/LDH)_{300}$ film.

may be aggravated in the presence of an implant material.[29] The results obtained for hemolysis of cells in presence of the (HEP/LDH)$_{300}$ film was 0.67 ± 0.06%. The value was much lower than the permissible hemolysis level of 5%. Hence, it was concluded that the (HEP/LDH)$_n$ film might be suitable as a biomaterial for specific application purposes.

Fig. 5 shows the clotting time curves for the (HEP/LDH)$_{300}$ film coated on Si and uncoated Si. Measurement of the clotting time was conducted to test the activated degree of intrinsic coagulation factors. The red blood cells were not entrapped in the formed thrombus that was hemolized and the free hemoglobin was dispersed in the solution. The concentration of the free hemoglobin in the resulting solution was measured colorimetrically.[23] As seen in Fig. 5, the optical densities were always bigger for the (HEP/LDH)$_{300}$-coated Si specimen than uncoated Si no matter how long the blood was in contact with the materials. A boundary condition could be defined when the optical density was 0.1, the corresponding time was the clotting time. It could be seen that the clotting time for HEP/LDH coating was 41.9 min, which was higher than that of the uncoated Si substrate (11.5 min). This indicated that heparin, as an anticoagulant medicament in the multilayer, could contribute a cruor retardant effect. Therefore the multilayer film was considered to have some thrombo resistant properties. As a result of the hemolysis and dynamic clotting time tests, the biocompatible material (HEP/LDH)$_n$ may prove to be beneficial for new medical applications.

Mechanical properties of the (HEP/LDH)$_n$ ultrathin film

Nanoindentation was used to measure the mechanical properties of the LDH/HEP composites. The data collected in the tests are displayed in figures (Fig. 6 and 7 and Fig. S1†), along with reduced modulus (E_r) values that were calculated from the load–displacement curves using the Oliver and Pharr approach.[30] To demonstrate full nanomechanical characterization of (HEP/LDH)$_{300}$ films, we used Hysitron's state-of-the-art TI 950 TriboIndenter, normal nanoindentation tests and a novel partial unloading (PUL) technique to obtain the results.

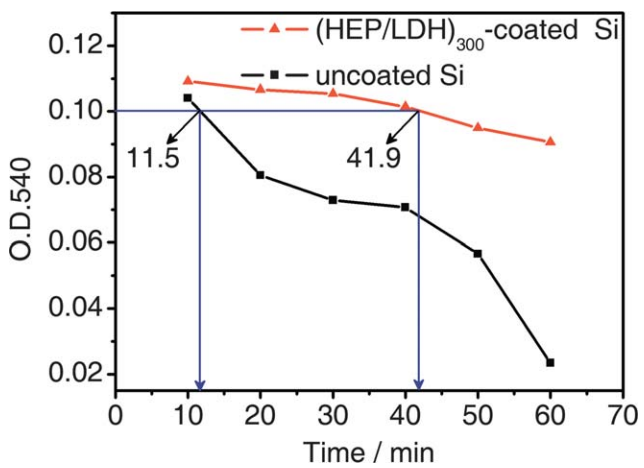

Fig. 5 A comparison of the blood-clotting profile for (HEP/LDH)$_{300}$-coated Si and uncoated Si.

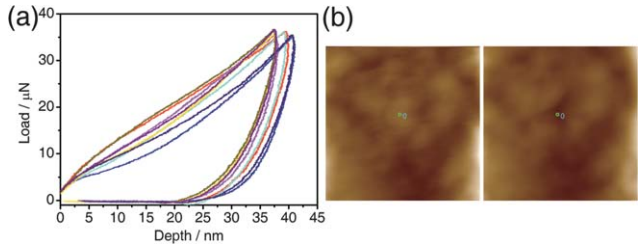

Fig. 6 (a) Force–displacement curves of nanoindentation tests on (HEP/LDH)$_{300}$ film. (b) 2 μm, 2-D topographical *in situ* SPM image of the sample surface after a 100 μN load-controlled nanoindentation test.

Nanoidentation test. A representative 2 μm 2-D topographical *in situ* SPM image showed surface characterization of the film, the location of indents could be accurately set (marked in left part of Fig. 6b) to ensure site-specific indentation. After a 100 μN load-controlled nanoindentation test, another representative 2 μm 2-D topographical *in situ* SPM image was taken (right part of Fig. 6b). It showed a triangular mark caused by the Berkovoich indenter in the previously marked site-specific area. Examination of the area surrounding the indentation revealed no crack formation at the corners of the mark. Similar post-indentation images were captured for each nanoindentation test to ensure the indents were performed in desired locations. From Fig. 6a, the result is not impacted with the mild creep of the initial part of unload curve. The mechanical properties of (HEP/LDH)$_{300}$ (E_r = 22.27 ± 0.81 GPa) were measured by nanoindentation.

PUL test. PUL enabled depth-profiling of the film by performing multiple partial unloads followed by reloading to a greater maximum load during a single test, based on ref. 31. Three PUL indents (Fig. 7 and Fig. S1, ESI†) on each sample were used to determine the hardness and reduced elastic modulus of the film as a function of thickness. One of the PUL test results can be seen in Fig. 7a. A representative 2 μm 2-D topographical

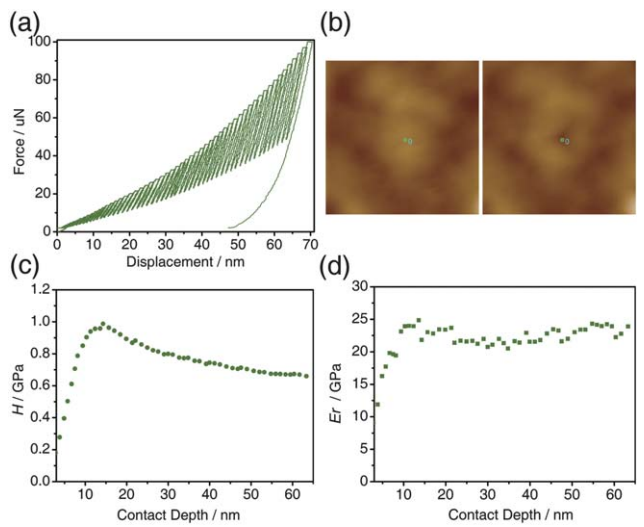

Fig. 7 The PUL test made on the (HEP/LDH)$_{300}$ film. (a) Load displacement profile obtained by a PUL test. (b) 2 μm, 2-D topographical *in situ* SPM image of the sample surface. (c) Hardness of the (HEP/LDH)$_{300}$ film. (d) The modulus values of the sample.

in situ SPM image was obtained on the film after a PUL test (Fig. 7b). Compared with the obtained *in situ* SPM images, the force of the nanoindentation test could not initiate crack formation. Two different regions were observed (Fig. 7c and d): (i) in the region at low penetration depth values, both H and E_r of the coating increased sharply at first, and then gradually to a maximum value with increasing indentation depth (until 15 nm), indicating that the mechanical properties were highly dependent on superficial roughness and the curvature radius of probe, and (ii) in the region at high penetration depths, the E_r remained constant for penetration depths higher than 15 nm, while H showed a slightly decreasing trend as a function of indenter contact depth. Because the influence of the elastic deformation range far outweighed the plastic area for the determination of E_r 22.48 $\pm$ 1.09 GPa (modulus values were calculated from the load–displacement curves using standard techniques), influence from the substrate was unavoidable. No cracks were found around the indent in the residual SPM image. The PUL nanoindentation data showed excellent agreement between the different nanoindentation methods. The modulus of the $(HEP/LDH)_{300}$ ultrathin film reached *ca.* 23 GPa. The value was twice and five times larger than for a $(PVA/LDH)_n$[17] film and a $(chitosan/LDH)_n$[10] film, respectively. Each HEP molecule contained *ca.* 20 sulfonic groups and *ca.* 10 carboxylic groups which gives it much stronger electrostatic interactions with the positively charged LDH monolayers to form a high orderly multilayered structure with nanometer-level control. Furthermore, a great number of hydroxy groups on the surface of LDH nanoplatelets as well as in the HEP molecules would facilitate the formation of a hydrogen bond network at the organic–inorganic interface. Therefore, a high level of ordering of the nanoscale building blocks, combined with strong electrostatic interactions and hydrogen bonding led to effective load transfer between nanosheets and the polymer.

Conclusions

In summary, we have developed a novel ultrathin film for mimicking nacre with regular structure by bottom–up LBL deposition of renewable LDH nanoplatelets and natural HEP *via* strong electrostatic attraction. The obtained bionanocomposite film had an orderly brick-and-mortar microstructure, which led to high performance mechanical properties and blood compatibility. The mechanical performance (modulus to 23 GPa) of the obtained $(HEP/LDH)_n$ artificial material is better than previously reported polymer-LDH hybrid films. Due to the interlamellar heparin, the $(HEP/LDH)_{300}$ film hemolysis value was much lower than the permissible level and dynamic clotting time was simultaneously prolonged. Further extension of the present strategy is expected to allow access to a variety of regular nacre-like ultrathin films with high mechanical properties and multifunctionality.

Acknowledgements

The authors are thankful for financial support from the National Basic Research Program of China (2010CB934700).

Notes and references

1 L. Addadi and S. Weiner, *Nature*, 2001, **411**, 753–755.
2 Z. Y. Tang, Y. Wang, P. Podsiadlo and N. A. Kotov, *Adv. Mater.*, 2006, **18**, 3203–3224.
3 P. Podsiadlo, E. M. Arruda, E. Kheng, A. M. Waas, J. Lee, K. Critchley, M. Qin, E. Chuang, A. K. Kaushik, H. S. Kim, Y. Qi, S. T. Noh and N. A. Kotov, *ACS Nano*, 2009, **3**, 1564–1572.
4 A. Zhuk, R. Mirza and S. Sukhishvili, *ACS Nano*, 2011, **5**, 8790–8799.
5 Q. Zhao, J. W. Qian, Q. F. An and B. Y. Du, *J. Mater. Chem.*, 2009, **19**, 8448–8455.
6 A. Walther, I. Bjurhager, J. M. Malho, J. Pere, J. Ruokolainen, L. A. Berglund and O. Ikkala, *Nano Lett.*, 2010, **10**, 2742–2748.
7 Z. Y. Tang, N. A. Kotov, S. Magonov and B. Ozturk, *Nat. Mater.*, 2003, **2**, 413–418.
8 P. Podsiadlo, Z. Q. Liu, D. Paterson, P. B. Messersmith and N. A. Kotov, *Adv. Mater.*, 2007, **19**, 949–955.
9 H. B. Yao, H. Y. Fang, Z. H. Tan, L. H. Wu and S. H. Yu, *Angew. Chem., Int. Ed.*, 2010, **49**, 2140–2145.
10 H. B. Yao, Z. H. Tan, H. Y. Fang and S. H. Yu, *Angew. Chem., Int. Ed.*, 2010, **49**, 10127–10131.
11 H. Zhu, S. Huang, Z. Yang and T. X. Liu, *J. Mater. Chem.*, 2011, **21**, 2950–2956.
12 C. Zhang, W. W. Tjiu, W. Fan, Z. Yang, S. Huang and T. X. Liu, *J. Mater. Chem.*, 2011, **21**, 18011–18017.
13 S. Deville, E. Saiz, R. K. Nalla and A. P. Tomsia, *Science*, 2006, **311**, 515–518.
14 P. Podsiadlo, A. K. Kaushik, E. M. Arruda, A. M. Waas, B. S. Shim, J. D. Xu, H. Nandivada, B. G. Pumplin, J. Lahann, A. Ramamoorthy and N. A. Kotov, *Science*, 2007, **318**, 80–83.
15 L. J. Bonderer, A. R. Studart and L. J. Gauckler, *Science*, 2008, **319**, 1069–1073.
16 E. Munch, M. E. Launey, D. H. Alsem, E. Saiz, A. P. Tomsia and R. O. Ritchie, *Science*, 2008, **322**, 1516–1520.
17 J. B. Han, Y. B. Dou, D. P. Yan, J. Ma, M. Wei, D. G. Evans and X. Duan, *Chem. Commun.*, 2011, **47**, 5274–5276.
18 Z. P. Liu, R. Z. Ma, M. Osada, N. Iyi, Y. Ebina, K. Takada and T. Sasaki, *J. Am. Chem. Soc.*, 2006, **128**, 4872–4880.
19 F. Mi, X. T. Chen, Y. W. Ma, S. T. Yin, F. L. Yuan and H. Zhang, *Chem. Commun.*, 2011, **47**, 12804–12806.
20 C. M. Jiao, Z. Z. Wang, Z. Ye, Y. Hu and W. C. Fan, *J. Fire Sci.*, 2006, **24**, 47–64.
21 D. P. Yan, J. Lu, M. Wei, J. B. Han, J. Ma, F. Li, D. G. Evans and X. Duan, *Angew. Chem., Int. Ed.*, 2009, **48**, 3073–3076.
22 S. Huang, H. D. Peng, W. W. Tjiu, Z. Yang, H. Zhu, T. Tang and T. X. Liu, *J. Phys. Chem. B*, 2010, **114**, 16766–16772.
23 Y. Imai and Y. NOSE, *J. Biomed. Mater. Res.*, 1972, **6**, 165–172.
24 K. Kaifu and T. Komai, *J. Biomed. Mater. Res.*, 1982, **16**, 757–766.
25 T. Kawasaki and T. Komai, *J. Biomed. Mater. Res.*, 1985, **19**, 851–861.
26 T. Hibino and W. Jones, *J. Mater. Chem.*, 2001, **11**, 1321–1323.
27 T. Hibino, *Chem. Mater.*, 2004, **16**, 5482–5488.
28 R. J. Sommer, M. Recto, R. J. Golinko and R. B. Griepp, *Circulation*, 1996, **94**, 249–252.
29 R. K. Dey and A. R. Ray, *Biomaterials*, 2003, **24**, 2985–2993.
30 W. C. Oliver and G. M. Pharr, *J. Mater. Res.*, 1992, **7**, 1564–1583.
31 X. D. Li, W. C. Chang, Y. J. Chao, R. Z. Wang and M. Chang, *Nano Lett.*, 2004, **4**, 613–617.

